Research Square

Preprints are preliminary reports that have not undergone peer review.
They should not be considered conclusive, used to inform clinical practice,
or referenced by the media as validated information.

Projection and Spatiotemporal Analysis of the Fire Weather Index (FWI) across Iran's Vegetation Regions under Climate Change

Mahmoud Ahmadi

maclimatology@gmail.com

Shahid Beheshti University

Kobra Shojaeizaedeh Postdoc

Shahid Beheshti University

Research Article

Keywords: climate change, CMIP6, fire weather index, forest fire, Iran's vegetation regions

Posted Date: November 20th, 2026

DOI: https://doi.org/10.21203/rs.3.rs-11388937/v1

License: This work is licensed under a Creative Commons Attribution 4.0 International License.
Read Full License

Additional Declarations: No competing interests reported.

Projection and Spatiotemporal Analysis of the Fire Weather Index (FWI) across Iran's Vegetation Regions under Climate Change

Mahmoud Ahmadi*

Associate Professor, Department of Physical Geography, Faculty of Earth Sciences, Shahid Beheshti University, Tehran, Iran, Postal Code: 1983969411 (Corresponding author: maclimatology@gmail.com)

Kobra Shojaeizaedeh

Postdoc reasercher, Department of Physical Geography, Faculty of Earth Sciences, Shahid Beheshti University, Tehran, Iran, Postal Code: 1983969411 (ghaderi.f41@gmail.com)

Projection and Spatiotemporal Analysis of the Fire Weather Index (FWI) across Iran's Vegetation Regions under Climate Change

Abstract

Climate change is a gradual process whose effects on wildfire-danger patterns in forests and rangelands may become apparent over several decades. This study aimed to assess spatiotemporal changes in the Fire Weather Index (FWI) across Iran's vegetation regions under SSP2-4.5 and SSP5-8.5 during the near future (2026–2050) and far future (2076–2100). Air temperature, relative humidity, precipitation, and wind speed from 69 synoptic meteorological stations and 16 climate models were examined for the baseline (1990–2014) and projection (2026–2100) periods. Model performance was evaluated using RMSE, MAE, r, and |Bias|. An ensemble of the 16 models was developed using the Independence-Weighted Mean (IWM) method. Results showed that the ensemble outperformed individual models. FWI was then calculated from the climatic variables, validated against burned-area data using Spearman's rank correlation coefficient, and its spatial and temporal changes across Iran's vegetation regions were evaluated. Under both future scenarios, FWI values would increase in all vegetation regions relative to the historical period.The magnitude varied spatially and temporally among scenarios and vegetation regions, with the highest index values projected under high-emissions SSP5-8.5, particularly in the far future. The largest increases were projected for the Khalij-Omani and Irano-Turanian regions. Zagros, Hyrcanian, and Arasbaran also showed substantial upward trends relative to the historical period. Summer is projected to remain the most critical season for fire danger. However, the greatest percentage change in FWI was estimated for winter (45.5%), followed by spring (22.1%), indicating that fire-conducive weather conditions may extend into colder and transitional seasons.

Keywords: climate change; CMIP6; fire weather index; forest fire; Iran's vegetation regions

1. Introduction

Wildfires in forests and rangelands are among the most consequential natural hazards, affecting not only ecosystem and forest functioning but also the health and safety of human communities (Bolan et al., 2025; Ndalila et al., 2024). By the end of the twenty-first century, climate change is expected to alter wildfire regimes and promote larger and

more severe fires, particularly at northern latitudes (Haas et al., 2026). Wildfires can reduce the resilience and recovery capacity of forest ecosystems, and this vulnerability is expected to increase under a changing climate (Lucas-Borja et al., 2025). Climate change raises air temperatures, especially during the dry season, thereby increasing evaporation and drying the soil surface. At the same time, decreasing precipitation and the increasing frequency of dry years and droughts create conditions that favor wildfire occurrence. Consequently, the frequency, severity, and duration of the fire season are projected to increase (Jolly et al., 2015). Indeed, major wildfires in recent years in Australia (Abram et al., 2021), Türkiye (Türkan et al., 2023), Greece (Koulelis et al., 2023), and Siberia (Novenko et al., 2023) have been attributed in part to anthropogenic climate change. Nevertheless, because geographical and environmental conditions differ, the influence of climate change on wildfires varies among regions.

Changes in climatic variables are expected to increase fire frequency and intensify fire-weather conditions, and thus fire danger, by the end of the twenty-first century (Miller et al., 2024). Projecting fire-conducive conditions and providing early warnings are therefore essential for fire prevention. In fire-danger assessment, meteorological variables are converted into relatively simple indices that can be used to estimate fuel moisture and, consequently, fire occurrence, behavior, and impacts (Stocks et al., 1989). One of the most widely used fire-danger indices is the Canadian Fire Weather Index (FWI), introduced in 1971 as part of the Canadian Forest Fire Danger Rating System (Van Wagner & Pickett, 1985). The FWI characterizes fire danger in terms of ignition potential and fire behavior, energy release, and rate of spread (San-Miguel-Ayanz & Ravail, 2005). Numerical fire-danger prediction models, rather than observations alone, can provide useful early-warning information one to two weeks in advance (Di Giuseppe et al., 2016). Because rising greenhouse-gas concentrations are expected to exacerbate fire-conducive conditions, resulting in more severe fires and larger burned areas (Li et al., 2021), future FWI projections commonly rely on outputs from the Coupled Model Intercomparison Project (CMIP), currently in its sixth phase (CMIP6) (Eyring et al., 2016). Moreover, the distributions of important drivers such as population and land cover will differ between present and future conditions; projections of forest-fire danger based on climate scenarios may therefore be affected by climate-model uncertainty (Ruosteenoja & Jylha, 2021). An ensemble of bias-corrected CMIP6 models can nevertheless reduce this uncertainty and improve the monitoring and projection of forest-fire danger.

Studies of the role of climate change in wildfires have demonstrated a direct association between higher air temperatures and both increased fire frequency and expansion of burned area (Flannigan et al., 2013; Tian et al., 2016; Dupuy et al., 2020). Numerous studies in Australia, Europe, the Iberian Peninsula, and the United Kingdom have also shown that climate-driven declines in fuel moisture lengthen the fire season and increase the number of days with high fire danger (Hennessy et al., 2005; De Rigo et al., 2017; Calheiros et al., 2020; Arnell et al., 2021). Fire danger and

wildfire severity are therefore expected to increase in many regions. Recent studies have accordingly examined future fire danger under various climate-change scenarios. As noted above, however, the inherent uncertainty of climate models introduces uncertainty into future fire-danger projections. Using 16 climate models, Gallo et al. (2022) found that the multi-model ensemble mean represented variability, magnitude, and spatial extent of fire danger more effectively than individual models at the global scale, while the performance of individual climate models remained strongly dependent on region and season. Li et al. (2024) likewise reported that although most CMIP6 models outperform CMIP5 models in estimating burned area and fire-related carbon emissions and in representing spatiotemporal fire patterns, they still face limitations in reproducing fire events. Matteo et al. (2025) examined a further limitation of CMIP6-based FWI calculation. The Canadian FWI requires meteorological observations at local noon, whereas climate models often provide only daily aggregate data, complicating accurate FWI calculation in climate-change studies. Thus, although existing evidence points to a potential increase in fire danger across many regions, model limitations can introduce considerable uncertainty into future projections.

Because the Canadian FWI is widely used to examine forest and rangeland fire danger, recent research has increasingly evaluated the index using simulations from CMIP6. Pereira et al. (2024) projected an increase in days with very high to extreme fire danger under all scenarios in Portugal, especially in southern and northeastern areas. CMIP6-based projections for India by Barik and Baidya Roy (2023) likewise confirmed that higher future temperatures are likely to increase FWI. In Greece, significant increases in FWI and longer periods of fire-conducive weather are expected, particularly in the south (Politi et al., 2023). Assessments across Europe and North Africa indicate substantial intensification and expansion of fire-conducive conditions, particularly under high-emissions scenarios (Di Nunno & Granata, 2025). Consistent with these findings, a study across Eurasia projected a 15-25% increase in fire-danger indices and longer fire seasons in the coming decades, driven mainly by higher temperatures and declining relative humidity (Tian et al., 2025). Research in the boreal forests of northeastern China further suggests that fire danger could increase by as much as 57% under high greenhouse-gas emissions, especially in summer (Debulois et al., 2026). To minimize the adverse effects of climate change in such fire-prone regions, fire prevention and management must increasingly be informed by rigorous assessments of future conditions. In Iran, previous studies have largely examined climatic and biophysical controls on fire occurrence. The growing availability of satellite fire products has also supported the monitoring and detection of active fires and burned areas and the assessment of their spatiotemporal patterns. Although the relationship between climate change and forest fires has been investigated in selected Iranian vegetation regions (Roshan et al., 2024), these studies have generally been case-specific, and no comprehensive assessment of the long-term behavior of forest-fire danger throughout Iran based on climate-model outputs has yet

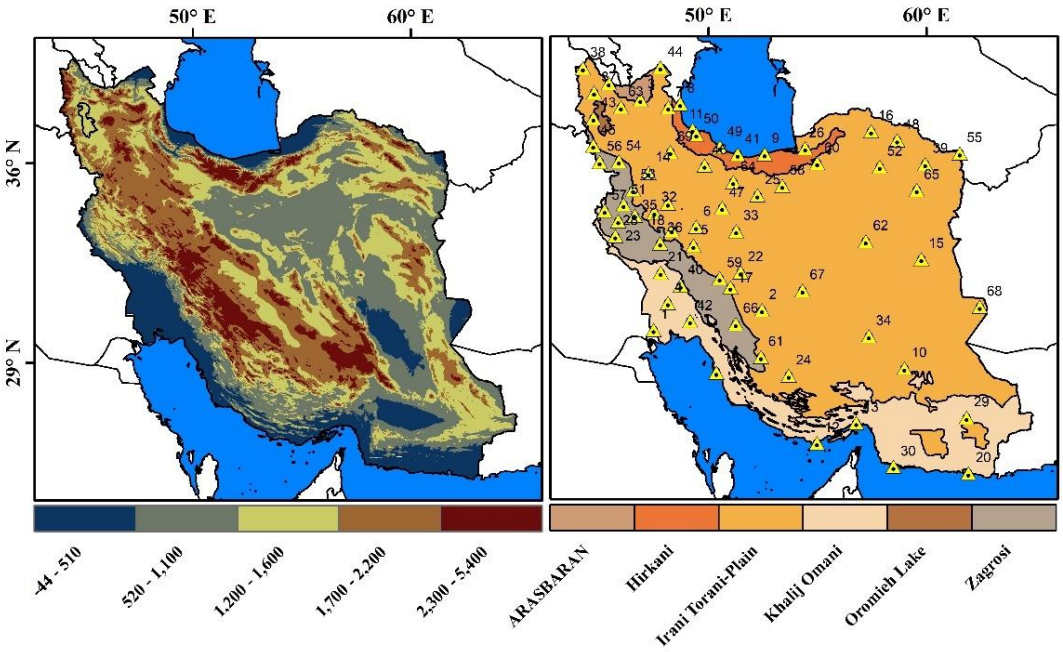
been presented. The present study therefore evaluates forest-fire danger across Iran's vegetation regions using climate-model simulations.

Iran is projected to experience an increase of 2.6 °C in mean air temperature and a 35% decrease in precipitation in the coming decades (Mansouri Daneshvar et al., 2019). According to World Bank data, Iran's total greenhouse-gas emissions, excluding land use, land-use change, and forestry (LULUCF), amounted to approximately 1.05 billion tonnes of carbon-dioxide equivalent (CO_2e) in 2024 (World Bank, 2026). If the projected climatic changes materialize, climate change will become a major driver of increasing fire danger and burned-area extent across Iran's vegetation regions. Given the recurrence of wildfires in different parts of the country, estimating fire danger, examining its spatiotemporal variability, and identifying the relevant climatic and biophysical controls can contribute to the prediction of fire regimes, preparation of fire-danger maps, and planning and management of high-risk areas. Because climate change is expected to substantially affect forest and rangeland fire danger in Iran, the principal objectives of this study were to (i) investigate spatiotemporal variations in fire danger across Iran's vegetation regions using the FWI, (ii) evaluate the relationship between FWI and burned area, (iii) assess future changes in fire danger using CMIP6 outputs under different greenhouse-gas emissions scenarios, and (iv) identify areas likely to become fire-prone in the future.

2. Materials and Methods

2.1. Study Area

The study area encompasses the entire territory of Iran. Iran's location within the world's arid and semi-arid belt, together with the prevailing meteorological and biophysical conditions, favors the occurrence and spread of fires in forests and rangelands. To examine the spatial pattern of fire danger, geospatial data for Iran's five principal vegetation regions - Hyrcanian, Irano-Turanian, Arasbaran, Khalij-Omani, and Zagros - were obtained from the Natural Resources and Watershed Management Organization of Iran, and the area of each region was calculated. Of the total area covered by these vegetation regions, the Hyrcanian region accounts for 2.81%, the Irano-Turanian region for approximately 71.82%, Arasbaran for approximately 0.63%, Khalij-Omani for 17.22%, and Zagros for approximately 7.53%. The Irano-Turanian region is therefore the country's largest vegetation region, extending from northwestern Iran to the south (Figure 1). Pronounced climatic and topographic diversity across these five regions has produced contrasting patterns of vegetation, fuel type, and the spatial and temporal behavior of wildfires.



code	Station	code	Station	code	Station	code	Station	code	Station	code	Station
1	Abadan	13	Bandarabbas	25	Garmsar	37	Khoy	49	Ramsar	61	Shiraz
2	Abadeh	14	Bijar	26	Gorgan	38	Maku	50	Rasht	62	Tabas
3	Ahar	15	Birjand	27	Hamedan	39	Mashhad	51	Ravansar	63	Tabriz
4	Ahvaz	16	Bojnoord	28	Ilam	40	Masjedsoleyman	52	Sabzevar	64	Tehran
5	Aligudarz	17	Borujen	29	Iranshahr	41	Nowshahr	53	Sanandaj	65	Torbat-E Heydariyeh
6	Arak	18	Borujerd	30	Jask	42	Omidiyeh	54	Saqez	66	Yasuj
7	Ardebil	19	Bushehr	31	Jolfa	43	Orumiyeh	55	Sarakhs	67	Yazd
8	Astara	20	Chahbahar	32	Kangavar	44	Parsabad	56	Sardasht	68	Zabol
9	Babolsar	21	Dezful	33	Kashan	45	Piranshahr	57	Sarpol-E-Zahab	69	Zanjan
10	Bam	22	Esfahan	34	Kerman	46	Qazvin	58	Semnan		
11	Bandar-E-Anzali	23	Eslamabad-E-Gharb	35	Kermanshah	47	Qom	59	Shahrekord		
12	Bandar-E-Lengeh	24	Fasa	36	Khorramabad	48	Quchan	60	Shahrud		

Figure 1. Geographical distribution of Iran's vegetation regions, elevation, and the meteorological stations used in the study.

2.2. Data

This study used multiple datasets to analyze the spatiotemporal pattern of fire danger across Iran's vegetation regions. Observations from the country's synoptic meteorological stations were used to validate the climate-model data. Climate-model outputs were then used to calculate FWI and assess future changes in fire danger across the vegetation regions. The FireCCI burned-area product was used to evaluate the performance of FWI during the historical period.

2.2.1. Meteorological Station Data

Daily air temperature, relative humidity, wind speed, and precipitation observations from 69 synoptic meteorological stations were used to validate the downscaled NEX-GDDP data. The stations were selected to ensure adequate spatial coverage of all vegetation regions, a common observation period, and minimal missing data. Consistent with the

historical period of the CMIP6 models evaluated in this study, the station records covered 1990-2014. The spatial distribution of the stations is shown in Figure 1.

2.2.2. NASA Earth Exchange Global Daily Downscaled Projections (NEX-GDDP)

The NASA Earth Exchange Global Daily Downscaled Projections (NEX-GDDP) dataset was developed by NASA as an enhanced, downscaled CMIP6 product. It comprises simulations from 35 models at a spatial resolution of 0.25° (approximately 25 km), providing substantially greater spatial detail than the original CMIP6 models, whose typical resolution is approximately 100 km or coarser (Thrasher et al., 2022). Historical and future projections are available for 1950-2100. NEX-GDDP uses the Bias-Correction Spatial Disaggregation (BCSD) method to correct and downscale CMIP6 output, thereby bridging the gap between coarse-resolution model simulations and the spatial detail required for impact studies (Jain et al., 2019). BCSD is implemented in two stages. First, quantile-mapping bias correction aligns the distributions of general circulation model (GCM) outputs with historical observations and removes systematic errors. Second, the corrected data are spatially interpolated onto a 0.25° grid (Table1).

To calculate FWI, daily air temperature, precipitation, relative humidity, and wind speed were obtained for the historical period (1990-2014) and two future periods - near term (2026-2050) and far future (2076-2100) - under the SSP2-4.5 and SSP5-8.5 scenarios. Data for 16 climate models were acquired from the NEX-GDDP-CMIP6 archive. These scenarios were selected to support a broader assessment of climate-change vulnerability and possible responses. Model selection at a horizontal resolution of 0.25° was based on the availability of all variables required to calculate FWI. Most of the selected models have also been used in recent CMIP6-based studies of fire-danger indices (Gallo et al., 2023; Debulois et al., 2025; He et al., 2025).

Table1.List of the 16 CMIP6 climate models used in this study

Model	Model
ACCESS-CM2	KACE-1-0-G
CESM2	MIROC6
CMCC-ESM2	MIROC-ES2L
GFDL-ESM4	MPI-ESM1-2-LR
HadGEM3-GC31-LL	MRI-ESM2-0
IITM-ESM	NorESM2-MM
INM-CM4-8	UKESM1-0-LL
INM-CM5-0	IPSL-CM6A-LR

2.2.3. Global Burned-Area Product (FireCCI 5.1.1)

Fire-danger indices estimate the likelihood of fire-conducive conditions from climatic variables. Their validity and performance must therefore be evaluated against observed fire outcomes. For this purpose, the FireCCI 5.1.1 dataset, developed under the European Space Agency's Climate Change Initiative (CCI), was used. The gridded burned-area product has a spatial resolution of 0.25° and a monthly temporal resolution. Data for 2001-2014 were analyzed in this study.

2.3. Methods

2.3.1. Canadian Fire Weather Index (FWI)

The well-established relationship between weather and wildfire has led to the development of numerous meteorology-based indices describing fire-weather conditions and, consequently, fire danger in different parts of the world. One of the most widely used is the Canadian Fire Weather Index (FWI), introduced in 1971 as part of the Canadian Forest Fire Danger Rating System (Van Wagner & Pickett, 1985). FWI is calculated daily from 2-m air temperature, relative humidity, precipitation, and 10-m wind speed (Van Wagner, 1987) (Figure 2). The system first calculates fuel-moisture codes and fire-behavior indices, which are then combined to obtain the final FWI value. Under the classification adopted by the European Forest Fire Information System (EFFIS), FWI values are commonly assigned to six danger classes (Figure 3), representing progressively greater probabilities of fire occurrence and spread. Because FWI integrates the components of the Canadian Forest Fire Danger Rating System (CFFDRS), it was selected as the principal variable for evaluating forest-fire danger in Iran. The FWI was calculated in R using the cffdrs package (Wang et al., 2017).

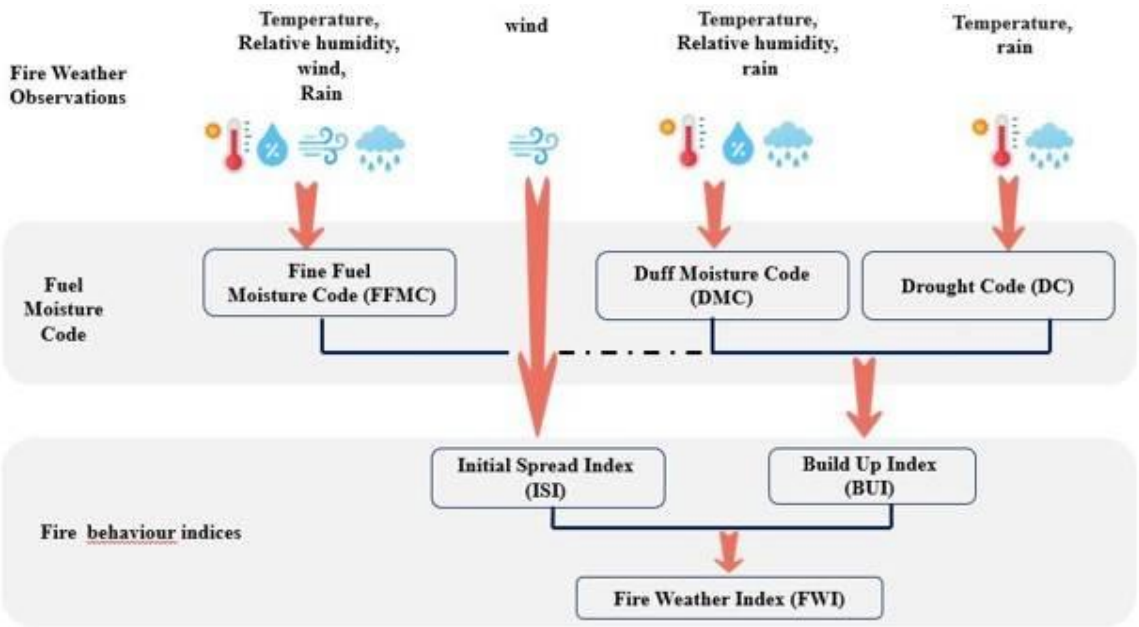


Figure 2. Structure and components of the Canadian Fire Weather Index system.



Figure 3. EFFIS classification of Fire Weather Index values.

2.3.2. Evaluation of CMIP6 Model Performance

Four statistical metrics were used to validate the selected NEX-GDDP models: root mean square error (RMSE), Pearson's correlation coefficient (r), mean absolute error (MAE), and absolute bias (|Bias|). RMSE quantifies the overall discrepancy between simulated and observed values, whereas MAE represents the mean magnitude of the errors. Pearson's correlation coefficient measures the strength of the linear relationship between simulated and observed values. Absolute bias was used to quantify systematic deviation of simulated values from observations. In the equations, X_i denotes the observed value, Y_i the model-simulated value for the corresponding month and station, and N the number of monthly observations used to calculate each metric. Overall performance metrics for each model were calculated from monthly data recorded at 71 stations during 1990-2014. Each model output was compared with the corresponding observations, and model performance was assessed using the four metrics. The ranks obtained for the four metrics were then summed to calculate a Final Score, on the basis of which the models were ranked.

Table 2. Statistical metrics used to validate the CMIP6 models.

Statistical metric	Equation
Root mean square error (RMSE)	$RMSE = \sqrt{\frac{\sum_{i=1}^{N}(X_i - Y_i)^2}{N}}$
Mean absolute error (MAE)	$MAE = \frac{\sum_{i=1}^{N}\lvert X_i - Y_i\rvert}{N}$
Absolute bias (|Bias|)	$\lvert Bias\rvert = \left\lvert \frac{1}{N}\sum_{i=1}^{N}(Y_i - X_i)\right\rvert$
Pearson's correlation coefficient (r)	$r = \frac{\sum_{i=1}^{N}(X_i - \bar{X})\,(Y_i - \bar{Y})}{\sqrt{\sum_{i=1}^{N}(X_i - \bar{X})^2 \sum_{i=1}^{N}(Y_i - \bar{Y})^2}}$

2.3.3. CMIP6 Multi-Model Ensemble Based on the IWM Method

The mean or a weighted combination of multiple models is commonly used to reduce uncertainty in climate projections. Ensemble approaches are founded on the assumption that independent errors tend to cancel one another (Tebaldi & Knutti, 2007). Climate projections from different models, however, cannot be considered fully independent. Bishop and Abramowitz (2013) developed the Independence-Weighted Mean (IWM) method, which characterizes inter-model dependence using the covariance of model errors. IWM is a linear combination of a set of model simulations that minimizes the mean squared deviation (MSD) from the observations. The method is expressed as follows:

$$\sum_{j=1}^{J}\left(\mu_e^j - y^j\right)^2 \quad (1)$$

$$\mu_e^j = \mathbf{w}^T\mathbf{x}^j = \sum_{k=1}^{K} w_k\, x_k^j \quad (2)$$

Here, j denotes the time step ($j = 1,2,\ldots,J$), k denotes the climate model ($k = 1,2,\ldots,K$), μ_e^j is the ensemble estimate at time step j, y^j is the observed value at that time step, w_k is the weight assigned to model k, and x_k^j is the value simulated by model k at time step j. A Lagrange multiplier was then used to impose the constraint $\sum_{k=1}^{K} w_k = 1$:

$$F(\mathbf{w},\lambda) = \frac{1}{2}\left[\frac{1}{J-1}\sum_{j=1}^{J}\left(\mu_e^j - y^j\right)^2\right] - \lambda\left(\sum_{k=1}^{K} w_k - 1\right)$$

(3)

The weight vector in Equation (3) was obtained as:

$$\mathbf{w} = \frac{\mathbf{A}^{-1}\mathbf{1}}{\mathbf{1}^{T}\mathbf{A}^{-1}\mathbf{1}}$$

(4)

where $\mathbf{1}^{T} = (1,1,\ldots,1)$ and $\mathbf{A}$ is the sample-based estimate of the covariance matrix of bias-corrected errors among all ensemble members:

$$\mathbf{A} = \frac{\sum_{j=1}^{J}\left(\mathbf{x}^{j} - y^{j}\right)\left(\mathbf{x}^{j} - y^{j}\right)^{T}}{J-1}$$

(5)

2.3.4. Relationship between FWI and Burned Area

The relationship between FWI and burned area was assessed seasonally over 2001-2014. Because the burned-area data contained many zero values and followed an asymmetric distribution, Spearman's rank correlation coefficient was used to evaluate the strength and direction of the association. The correlation coefficient (ρ) and its significance level (p-value) were calculated and reported for each season.

3. Results and Discussion

3.1. Validation and Performance Assessment of the Climate Models

The evaluation revealed clear differences among models and metrics, with performance also varying by climatic variable. INM-CM5-0 simulated relative humidity more accurately than the other models, exhibiting the smallest errors and the highest correlation coefficients relative to the observations. IPSL-CM6A-LR provided the best individual-model simulation of precipitation because it reproduced the observed precipitation patterns more effectively and yielded lower errors. Differences among models in the simulation of air temperature were comparatively small; nevertheless, UKESM1-0-LL performed best among the models evaluated. CESM2 provided the best overall simulation of wind speed. Wind speed, however, exhibited lower correlations and therefore greater uncertainty than the other climatic variables in most models, likely because of the complex processes governing near-surface wind (Figure 4). Thus, a different model performed best for each climatic variable: no single model was optimal for all variables, and model selection depended on both the variable and its climatic setting. This finding is consistent with Zabihi et al. (2024).

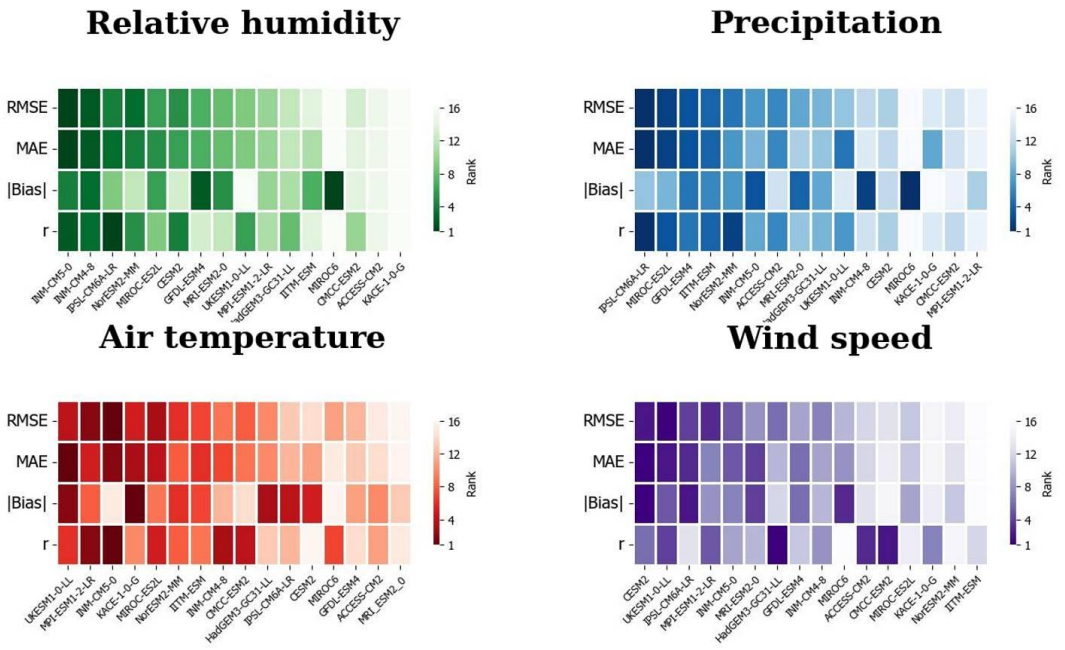


Figure 4. Performance ranks of the 16 climate models in simulating relative humidity, precipitation, air temperature, and wind speed.

Validation of the ensemble constructed using IWM showed that its performance relative to the best individual models varied with the climatic variable and evaluation metric. For relative humidity, MAE decreased from 12.25 for the best individual model (INM-CM5-0) to 8.75 for the ensemble. RMSE declined from 16.10 to 11.89 percentage points, while the correlation coefficient increased from 0.734 to 0.825. These results demonstrate the ensemble's ability to improve the simulation of relative humidity and reduce errors relative to the best individual model. Ensemble performance also improved markedly for precipitation: RMSE decreased from 52.39 to 29.89 mm month^{-1}, MAE declined from 25.59 to 14.24 mm month^{-1}, and the correlation coefficient increased from 0.305 to 0.607. Meng et al. (2025) similarly reported lower RMSE and higher correlation after combining climate models. The present results therefore indicate a substantial improvement in precipitation simulation and in the ensemble's capacity to represent observed precipitation variability. The superior performance of ensemble approaches relative to individual models has also been documented by Lei et al. (2023) in Central Asia and by Zarrin and Dadashi Roudbari (2022) in Iran.

The temperature results differed somewhat from those obtained for the other variables. Individual models already agreed closely with the observations during the baseline period, and the scope for further improvement through ensemble averaging was consequently limited. Azad and Ahmadi (2024) likewise noted that many CMIP6 models already simulate temperature effectively. RMSE and MAE for the best individual model, UKESM1-0-LL, were 2.67 and 2.05 °C, respectively. The corresponding ensemble values were 2.79 and 2.24 °C, indicating slightly larger RMSE and MAE. Nevertheless, the ensemble correlation coefficient (0.975) exceeded that of the individual model (0.964). Thus, the ensemble did not improve RMSE or MAE relative to the best individual temperature model, although it

produced a stronger correlation. Given the small differences in RMSE and MAE, the ensemble's overall temperature performance can be considered acceptable and close to that of the best individual model.

For wind speed, the ensemble reduced errors and improved the simulation. RMSE decreased from 1.86 to 1.39 m s^{-1}, MAE declined from 1.55 to 1.12 m s^{-1}, and the correlation coefficient increased from 0.152 for the best individual model to 0.239 for the ensemble, although the correlation remained low. These findings show that ensemble averaging reduced wind-speed simulation errors but produced only limited improvement in the representation of temporal variability. Weak correlations in simulated wind speed may be attributed to topography, local processes, and atmospheric stability, as discussed by Whittaker et al. (2025). Overall, the ensemble did not perform uniformly across climatic variables; its performance depended on both the variable and the evaluation metric. Ensemble assessment should therefore consider the type of variable and the full set of validation metrics simultaneously (Table 3).

Table 3. Performance of the best individual model and the IWM ensemble in simulating baseline climatic variables, 1990-2014.

Variable	Model	Bias	RMSE	MAE	r
Relative humidity	INM-CM5-0	-2.65	16.10	12.25	0.734
Relative humidity	IWM Ensemble	1.34	11.89	8.75	0.825
Precipitation	IPSL-CM6A-LR	-8.61	52.39	25.59	0.305
Precipitation	IWM Ensemble	-5.82	29.89	14.24	0.607
Air temperature	UKESM1-0-LL	-0.13	2.67	2.05	0.964
Air temperature	IWM Ensemble	-1.33	2.79	2.24	0.975
Wind speed	CESM2	1.22	1.86	1.55	0.152
Wind speed	IWM Ensemble	0.24	1.39	1.12	0.239

3.2. Performance of FWI in Identifying Fire-Prone Areas

The spatiotemporal distribution of burned area derived from the merged satellite product indicated a mean total burned area of 9 ha in winter, with values ranging from 0 to 5,302 ha. Burned area was generally limited in this season because of the prevailing climatic conditions. Fires were concentrated mainly in deciduous vegetation and montane forests, with the largest burned areas occurring southwest of the Caspian Sea and in parts of northwestern Iran. This pattern was associated with greater accumulations of dry biomass in these areas. Burned patches in the other vegetation regions were generally small, dispersed, and irregular. The mean winter FWI was 14.85, corresponding to moderate fire

danger. Among the vegetation regions, the largest mean values were recorded in Khalij-Omani (23.3) and Irano-Turanian (14.4). Winter precipitation, lower temperatures, and higher humidity placed the Zagros and Hyrcanian regions in the low-danger class, with mean values of 5.6 and 4.6, respectively. The occurrence of the highest FWI values in Khalij-Omani and Irano-Turanian, but the largest burned area in the Hyrcanian region and northwestern parts of Irano-Turanian, shows that vegetation and regional ecological characteristics operate alongside climatic controls. Nevertheless, FWI identified fire-conducive weather in a small part of Khalij-Omani, specifically the forests of Khuzestan, and classified it as high danger. As shown in Table 3, Spearman's analysis indicated a weak and statistically nonsignificant winter relationship between FWI and burned area.

In spring, mean total burned area increased to 12 ha and the maximum reached 6,434 ha. Burned areas were concentrated in the Khalij-Omani region of southwestern and western Iran. Spring precipitation promotes herbaceous growth, while rising temperatures - particularly late in the season - subsequently dry this vegetation and increase fire danger. Mean FWI across the country increased to 36.1, with a maximum of 62, indicating a marked intensification of fire-conducive weather. Mean FWI reached 48.7 in Khalij-Omani, 35.4 in Irano-Turanian, and 24.7 in Zagros, demonstrating the very high potential for fire-conducive weather in these regions. The Hyrcanian region, with a mean of 17.1, remained in the moderate-danger class. Overall, all Iranian vegetation regions except Arasbaran exhibited weather conditions conducive to fire in spring. FWI assigned the principal burned-area hotspot to a high-danger class, indicating its ability to identify a substantial share of the season's fire-prone areas. Correlation analysis also showed a positive and statistically significant relationship between FWI and burned area (Figure 5).

Mean burned area reached 174 ha in summer. Although the maximum burned area occurred in western and northwestern Iran, fires of varying severity and extent were distributed across all vegetation regions. Summer burned area ranged from 0 to 20,386 ha. Prevailing weather conditions increased FWI throughout the country: mean FWI was 53.7 and the maximum reached 71. The north-to-south increase in FWI and the widespread distribution of fires indicate that weather conditions conducive to fire prevailed across a substantial portion of Iran's vegetation regions. Many summer fires, however, are caused by human activities (Honareh et al., 2023). Human factors must therefore be considered alongside the decisive role of weather in managing summer fire danger in Iran. No significant contemporaneous association was found between FWI and burned area in summer (Spearman's $r = 0.11$). This result shows that higher FWI, particularly in summer, does not necessarily translate directly into a larger number of fires or greater burned area. Complete spatiotemporal correspondence between FWI and burned area cannot always be expected, because vegetation properties, human activity, and the availability of combustible fuel can strongly influence fire occurrence and spread (Jones et al., 2022). Because fires do not necessarily occur immediately after favorable

weather develops, part of the FWI signal may emerge after a time lag. A lag analysis was therefore conducted for summer. At lag 0, there was virtually no relationship. At lags 1 and 2 months, the relationships were weak, negative, and nonsignificant. Thus, even after introducing one- and two-month lags, no significant summer association was observed between FWI and burned area, indicating that FWI alone cannot explain summer burned-area variability (Table 5).

In autumn, mean total burned area was estimated at 42 ha and the maximum at 10,752 ha. The principal autumn burned-area hotspot was located in the Zagros region. Mean FWI was 28.8 and values ranged from 4 to 49. The onset of seasonal precipitation, declining temperature, and increasing relative humidity reduced the index. Nevertheless, the Khalij-Omani, Irano-Turanian, and Zagros regions remained in the high-danger class. Despite autumn precipitation, the Hyrcanian region, with a mean FWI of 14.3, was classified as moderate danger, while Arasbaran recorded the lowest mean FWI, at 4.2. FWI assigned the principal autumn burned-area hotspot to the high-danger class, demonstrating its ability to identify fire-conducive weather in the affected area. Spearman's analysis showed a positive and statistically significant autumn relationship between FWI and burned area.

Given the generally satisfactory ability of FWI to represent weather conditions relevant to fire occurrence across Iran's vegetation regions, the index was subsequently used to assess future fire danger under different climate-change scenarios.

Table 4. Seasonal Spearman correlations between FWI and burned area.

Season	Spearman's r	p-value
Spring	0.65	<0.001
Summer	0.11	0.47
Autumn	0.52	<0.001
Winter	0.27	0.085

Table 5. Summer lag analysis across Iran's vegetation regions.

Lag	Spearman's r	p-value
0 months	0.114	0.470
1 month	-0.027	0.890
2 months	-0.037	0.899

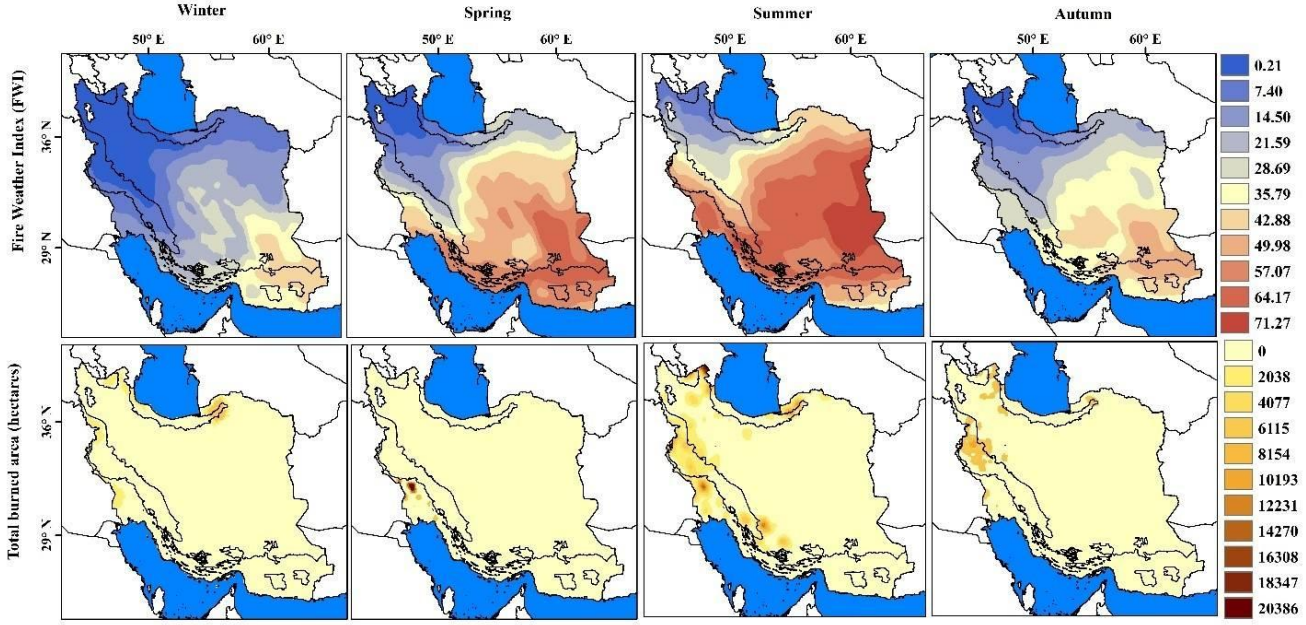


Figure 5. Seasonal FWI and burned area derived from the FireCCI product for 2001-2014.

3.3. Fire-Weather Danger during the Historical Period (1990-2014)

The historical mean FWI (1990-2014) indicated distinct danger classes across Iran. The highest seasonal mean occurred in summer (51.58), placing much of the country in the extreme-danger class. A gradual spring increase in temperature, earlier snowmelt, and a delayed onset of autumn precipitation may have contributed to mean FWI values of 35.84 in spring and 29.00 in autumn, creating weather conditions conducive to fire. The smallest seasonal mean, 14.81, was recorded in winter and corresponded to moderate danger. Summer and spring therefore encompassed the largest high-danger areas. Although fire danger decreased in autumn relative to summer and spring, dry areas in central, southern, and eastern Iran continued to exhibit high FWI values. High-danger areas became markedly more restricted in winter.

Across vegetation regions, the highest FWI values in all seasons occurred in Khalij-Omani, followed by Irano-Turanian. The highest seasonal means in these regions occurred in summer (58.76 and 54.40, respectively), largely because of their hot and dry climates, limited precipitation, and relatively sparse vegetation. The other vegetation regions also exhibited substantial summer increases relative to the other seasons. Although FWI values in Zagros, Arasbaran, and Hyrcanian were lower than those in Khalij-Omani and Irano-Turanian, these ecosystems are highly sensitive and critically important for biodiversity conservation, soil and water protection, and the provision of natural resources; their vulnerability is therefore considerable. The summer maximum was highest in Irano-Turanian (71.02), followed by Khalij-Omani (69.73). As shown in Table 5, the broad area, climatic diversity, and environmental heterogeneity of the Irano-Turanian region allowed low through extreme danger conditions to coexist in different parts

of the region. Higher mean and maximum values in every vegetation region confirm that summer is the most critical season for fire danger across Iran. The contrasting index values among regions further underscore the importance of the climatic characteristics of each vegetation zone (Table 6).

Table 6. Seasonal FWI values for Iran and its vegetation regions during the historical period.

Spatial unit	Statistic	Winter	Spring	Summer	Autumn
National	Mean	14.81	35.84	51.85	27.10
National	Maximum	39.35	61.68	71.02	49.07
National	Minimum	0.19	2.50	10.48	3.57
Irano-Turanian	Mean	14.42	35.22	54.40	28.74
Irano-Turanian	Maximum	38.83	61.68	71.02	48.00
Irano-Turanian	Minimum	0.19	2.51	10.48	3.64
Khalij-Omani	Mean	23.24	48.49	58.76	36.46
Khalij-Omani	Maximum	39.35	61.55	69.73	49.07
Khalij-Omani	Minimum	4.28	21.47	38.22	22.87
Zagros	Mean	5.50	24.41	49.74	23.74
Zagros	Maximum	16.31	47.67	67.78	37.20
Zagros	Minimum	0.46	6.51	24.07	9.80
Hyrcanian	Mean	4.50	16.87	32.39	14.48
Hyrcanian	Maximum	9.22	26.79	45.63	22.46
Hyrcanian	Minimum	0.73	5.52	16.98	5.13
Arasbaran	Mean	0.47	4.29	15.00	3.57
Arasbaran	Maximum	0.63	5.00	17.12	5.92
Arasbaran	Minimum	0.39	3.82	14.19	4.31

3.4. FWI under SSP2-4.5 in the Near and Far Future

The spatial distribution of mean FWI under SSP2-4.5 in the near-term period indicated that the highest seasonal mean would occur in summer (53.15), followed by spring (38.28), autumn (28.53), and winter (16.51). In the far future, the corresponding means would increase to 54.60, 41.10, 29.21, and 19.83, respectively. Relative to the historical period,

FWI would increase in every season and in both projection horizons. Summer retained the highest mean in both periods, confirming that it would remain the season with the most fire-conducive weather in Iran. The projected seasonal pattern also indicated an extension of the period of elevated fire danger. In addition to summer, which retained extreme fire danger, spring changed from high danger in the historical period to very high danger in the future. Although FWI increased in autumn and winter in both future periods, these seasons remained in their historical danger classes of high and moderate, respectively.

Maximum FWI values also increased under SSP2-4.5, with a stronger increase in the far future than in the near term. In 2076-2100, projected seasonal maxima reached 74.79 in summer, 65 in spring, 52 in autumn, and 45 in winter.

Analysis of temporal patterns and spatial changes at the vegetation-region scale showed that mean FWI under SSP2-4.5 would increase in both future periods relative to the historical baseline. This rise indicates an intensification of weather conditions conducive to fire across Iran's vegetation regions. The larger increase in 2076-2100 than in 2026-2050 suggests that persistent climate change would progressively alter and intensify fire-conducive weather at different spatial and temporal scales, although conditions would vary among vegetation regions. Summer would remain the most critical season. Every vegetation region was projected to exhibit higher summer FWI than in other seasons. Arasbaran, which remained in the low-danger class during the other seasons, would move into the moderate-danger class in summer. The increase in northwestern Iran could therefore reflect increasingly favorable weather for forest fires in this region.

The highest projected regional mean under SSP2-4.5 was 57.78 in the Khalij-Omani region during summer in 2076-2100. Within this region, southwestern Iran, particularly Khuzestan, exhibited the greatest climatic potential for fire occurrence. Irano-Turanian and Zagros followed, with summer means of 54.0 and 49.2, respectively. Because FWI increased throughout the Zagros region, the probability of fire under conducive weather conditions can be expected to rise. In the Hyrcanian region, especially the Golestan forests, summer fire danger was projected to reach the high-danger class (Figure 6). Because this area has repeatedly experienced fires in the past, an increase in FWI could increase the likelihood of fire whenever other necessary drivers are present. Given the ecological value of the Zagros, Hyrcanian, and Arasbaran regions, any fire in these areas threatens national natural assets, biodiversity, vegetation, environmental security, and the livelihoods of local communities.

Although the countrywide mean summer FWI did not increase sharply relative to the historical period, the persistence of extreme summer values indicates a likely expansion of fire-conducive conditions in space and time. Adequate preventive measures are therefore essential across all vegetation regions.

Under SSP2-4.5, spring fire-conducive weather was projected to intensify across most Iranian vegetation regions. The highest spring mean, 52.78, was projected for Khalij-Omani in the far future. Previous findings (Figure 5) showed that this region already sustains a substantial spring burned area; a future increase in FWI could therefore play an important role in regional forest fires. Despite increasing FWI in both future periods, the Zagros region would remain in the high-danger class in spring and autumn, as in the historical period. Mean FWI in the Hyrcanian region would increase relative to the historical period in both horizons, moving the region into the high-danger class. These results suggest that Iranian forests and rangelands, particularly those in mountainous areas, are likely to face greater climate-driven fire danger in the future.

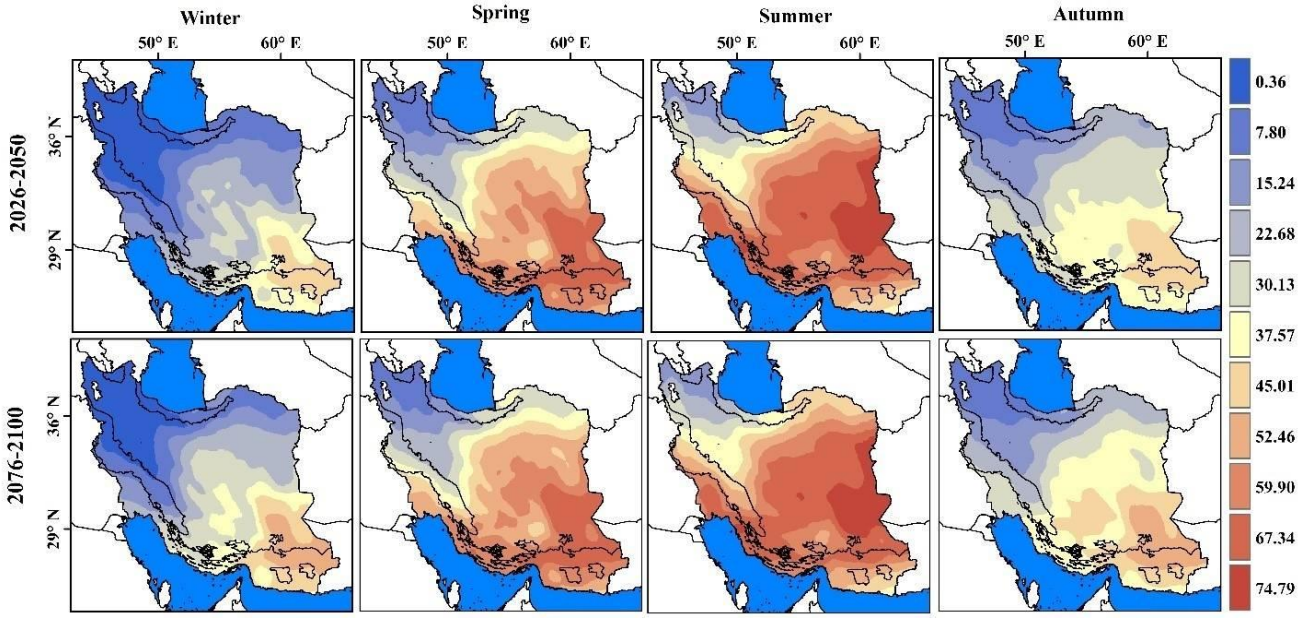


Figure 6. Spatiotemporal distribution of FWI under SSP2-4.5 for 2026-2050 and 2076-2100.

3.5. FWI under SSP5-8.5 in the Near and Far Future

Under SSP5-8.5, the narrowest seasonal range of FWI occurred in winter: values ranged from 1.5 to 43.4 in the near future and from 2.3 to 47.99 in the far future. In spring, the range increased from 3.95-64.33 in the near future to 6.15-67.13 in the far future. The widest range occurred in summer, from 12.98 to 76.49 in the near future and from 17.10 to 79.90 in the far future. Autumn values ranged from 4.85 to 49.29 in the near future and from 6.5 to 52.49 in the far future. The increase in the range of FWI in every season relative to the historical period indicates an intensification of fire-conducive weather across Iran's vegetation regions.

Seasonal mean FWI also increased relative to the historical period. In the near future, mean values for winter, spring, summer, and autumn were projected to reach 17.27, 39.57, 53.96, and 29.19, respectively; in the far future, the corresponding values were 21.55, 43.73, 55.34, and 30.47. The increase was therefore evident in both future periods.

The persistence of the highest and most critical fire danger in summer is consistent with projected climatic trends. CMIP6-based studies show that air temperature in Iran will increase under all climate scenarios, particularly SSP5-8.5, during summer (Ghazi et al., 2024). Together with declining relative humidity and increasingly dry vegetation, this warming is likely to increase FWI and exacerbate fire danger. Autumn remained in the high-danger class. Of particular importance, spring shifted from high to very high danger, while high-danger conditions expanded into winter in the far future. These changes would lengthen the fire-danger season across Iran.

At the vegetation-region scale, SSP5-8.5 produced an increase in mean FWI during both future periods relative to the historical baseline. This increase was not confined to a particular region; instead, all vegetation regions experienced an intensification of fire-conducive weather, although the magnitude varied. The results are consistent with Nogherotto et al. (2026), who identified rising temperature, declining relative humidity, and altered precipitation patterns as major drivers of future fire-weather intensification. The greatest increases in mean FWI were projected, in descending order, for Khalij-Omani, Irano-Turanian, Zagros, Hyrcanian, and Arasbaran.

Higher summer means in every vegetation region ensured that summer would remain Iran's most critical fire-danger season. The highest mean was projected for Khalij-Omani (59.11), while the lowest occurred in Arasbaran (21.80). Although Arasbaran retained the lowest FWI among the regions, its increase was sufficient to shift the region from moderate danger in the historical period to high danger in the future, thereby increasing the likelihood of fire. In the Zagros region, especially large increases were projected for summer and spring. In the Hyrcanian region, spring danger shifted from moderate (16.80) to high (23.90) in the far future. This shift indicates that, in addition to the continued prevalence of critical fire weather in Iran's hot and dry areas, mountainous regions would also experience more fire-conducive weather and potentially greater fire occurrence. The upward trend points to a lengthening of the fire-danger period and an expansion of high-danger areas under future climate scenarios.

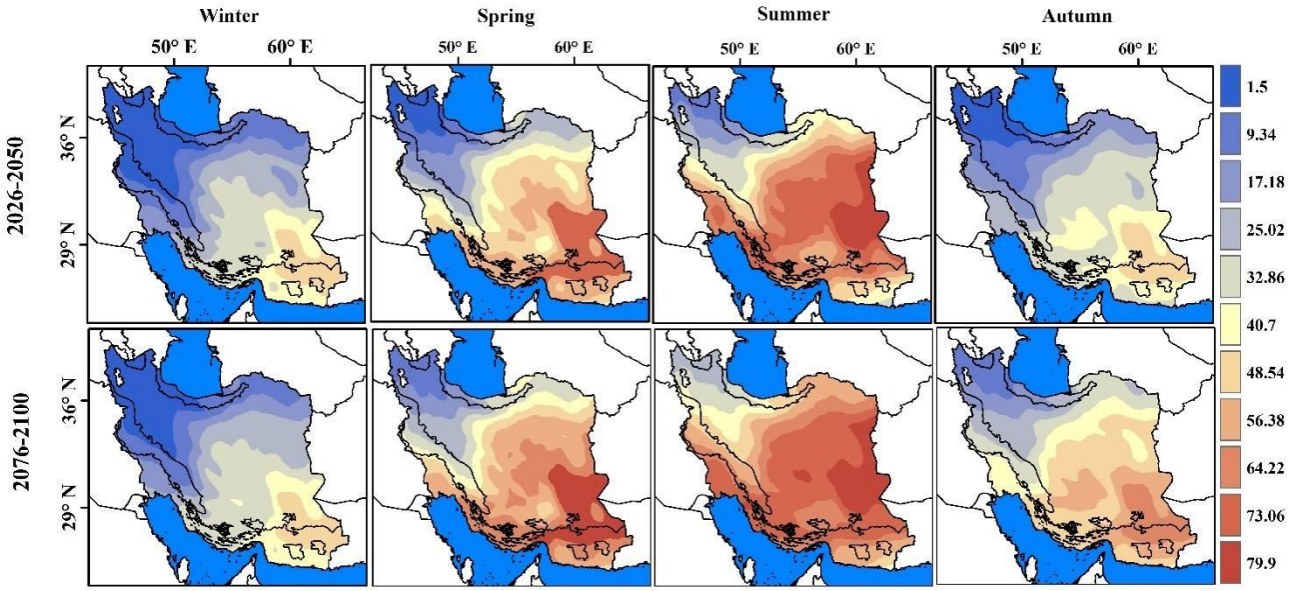


Figure 7. Spatiotemporal distribution of FWI under SSP5-8.5 for 2026-2050 and 2076-2100.

3.6. Distribution of High-Danger Areas during the Historical and Future Periods

Because the very high and extreme classes represent the greatest fire danger and the strongest potential for fire occurrence and spread, **FWI ≥ 38** was adopted as the threshold for classifying high-danger areas. During the historical period, summer encompassed the largest high-danger area: 83.28% of Iran was classified as very high or extreme danger (FWI ≥ 38). The Irano-Turanian and Khalij-Omani regions of central, southern, and eastern Iran accounted for the largest shares of the country's high-danger area, at 70.96% and 20.10%, respectively. This pattern is consistent with their high temperatures, low relative humidity, limited precipitation, and relatively strong winds, particularly in late spring and summer. The Zagros and Hyrcanian regions - the latter mainly represented by the Golestan forests - accounted for 7.78% and 1.16% of the country's high-danger area, respectively, whereas Arasbaran was almost entirely outside the high-danger zone in summer. The broad spatial distribution shows that fire-conducive conditions were not limited to central, southern, and eastern Iran but extended into western and mountainous areas.

After summer, spring had the largest high-danger area, covering 56.51% of Iran. Irano-Turanian, Khalij-Omani, and Zagros accounted for 71.25%, 27.32%, and 1.42% of this high-danger area, respectively. The national high-danger area declined to 13.58% in autumn and 0.39% in winter.

Table 7. Area and percentage of high-danger zones (FWI ≥ 38) across Iran during the historical and future periods.

Season	Metric	Historical	SSP2-4.5 2026-2050	SSP5-8.5 2026-2050	SSP2-4.5 2076-2100	SSP5-8.5 2076-2100
Winter	Area (km²)	6,317.60	26,080.36	44,709.18	113,716.80	157,778.10

Season	Metric	Historical	SSP2-4.5 2026-2050	SSP5-8.5 2026-2050	SSP2-4.5 2076-2100	SSP5-8.5 2076-2100
Winter	Percentage (%)	0.39	1.61	2.76	7.02	9.74
Spring	Area (km²)	915,404.44	980,848.82	1,009,196.54	1,047,589.13	1,115,699.87
Spring	Percentage (%)	56.51	60.55	62.30	64.67	68.85
Summer	Area (km²)	1,349,051.17	1,376,348.23	1,385,012.91	1,379,343.26	1,423,890.47
Summer	Percentage (%)	83.28	84.99	85.50	85.15	87.90
Autumn	Area (km²)	219,982.17	243,309.70	290,771.71	325,313.56	393,635.25
Autumn	Percentage (%)	13.58	15.02	17.95	20.07	24.30

The area exposed to high fire danger increased in every season and future period relative to the historical baseline. In other words, extensive portions of Iran would increasingly experience weather conducive to high fire danger. The spatial expansion of fire danger was greater in the far future than in the near term. Its magnitude and distribution, however, were not uniform across seasons or vegetation regions, reflecting differences in climate, vegetation, and other environmental conditions.

Under both SSP2-4.5 and SSP5-8.5, more than 80% of Iran was classified as very high or extreme danger (FWI ≥ 38) in summer. Under SSP5-8.5 at the end of the century, the high-danger area reached its maximum extent, covering 87.9% of the country and exposing a substantial portion of Iran to conditions favorable for fire ignition and spread. Spring exhibited the second-largest increase. The greatest expansion occurred in the far future under SSP5-8.5, when the national high-danger share increased from 83.28% in the historical period to 87.9%. Although increases in autumn and winter were smaller than those in the warmer seasons, they remained substantial relative to the historical period.

Despite the expansion of high-danger areas under the future scenarios, their spatial distribution among vegetation regions remained relatively stable, and most of the increase occurred in regions that had already dominated during the historical period. The Irano-Turanian region consistently accounted for a large share - generally more than 70% - of the country's high-danger area across seasons and scenarios. Its vast extent and predominantly arid to semi-arid climate keep it among the highest-danger regions. Khalij-Omani and Zagros contributed the next-largest shares. In some regions and seasons, however, no area reached FWI ≥ 38 (Table 7). Future projections for the forests of northern and northwestern Iran showed no very-high-danger area in Arasbaran, while the Hyrcanian region accounted for only a small fraction of the national high-danger area. These results suggest that even Iran's humid forests may face increasing fire danger under climate change, although some regions and seasons still exhibited no FWI values ≥ 38.

Table 8. Percentage contribution of each vegetation region to Iran's total high-danger area (FWI ≥ 38). Blank cells indicate that no area met the threshold.

Season	Period/scenario	Irano-Turanian	Zagros	Arasbaran	Hyrcanian	Khalij-Omani
Winter	Historical	91.39				8.60
Winter	SSP2-4.5 (2026-2050)	84.16				15.84
Winter	SSP5-8.5 (2026-2050)	25.16				74.83
Winter	SSP2-4.5 (2076-2100)	46.65				53.35
Winter	SSP5-8.5 (2076-2100)	50.06				49.94
Spring	Historical	71.25	1.42			27.32
Spring	SSP2-4.5 (2026-2050)	71.81	1.65			26.54
Spring	SSP5-8.5 (2026-2050)	71.99	1.72			26.27
Spring	SSP2-4.5 (2076-2100)	72.00	1.73			26.28
Spring	SSP5-8.5 (2076-2100)	72.43	2.90			24.67
Summer	Historical	70.96	7.78		1.16	20.10
Summer	SSP2-4.5 (2026-2050)	70.88	7.79		1.32	20.01
Summer	SSP5-8.5 (2026-2050)	70.94	7.78		1.39	19.87
Summer	SSP2-4.5 (2076-2100)	70.78	7.77		1.39	19.96
Summer	SSP5-8.5 (2076-2100)	71.84	7.80		1.42	19.92
Autumn	Historical	63.40				36.60
Autumn	SSP2-4.5 (2026-2050)	64.68				35.31
Autumn	SSP5-8.5 (2026-2050)	66.05				33.94
Autumn	SSP2-4.5 (2076-2100)	67.80				32.19
Autumn	SSP5-8.5 (2076-2100)	70.65	0.12			29.23

4. Conclusion

Wildfires arise from interactions among climatic conditions, topography, vegetation, and human activities, and the contribution of each factor varies geographically (Wu et al., 2021). Because climate change alters the weather conditions conducive to fire, this study examined spatial and temporal changes in fire-weather danger across Iran's vegetation regions using FWI under SSP2-4.5 and SSP5-8.5 for the near-term (2026-2050) and far-future (2076-2100) periods.

The results showed that climate change could intensify weather conditions conducive to fire and lengthen the fire-danger period across Iran's vegetation regions. Under both SSP2-4.5 and SSP5-8.5, FWI increased in every region relative to the historical period. The largest increases were projected for 2076-2100, particularly under SSP5-8.5, indicating an intensification of fire-conducive weather across many Iranian ecosystems and an expansion of high-danger conditions in both space and time. This finding is consistent with Carrillo et al. (2022), who reported higher FWI in the Canary Islands under SSP5-8.5 during 2077-2099.

At the seasonal scale, summer exhibited the greatest danger. The findings agree with Bento et al. (2023), who also reported higher summer FWI relative to the historical period. Nevertheless, increasing danger in spring and autumn and the extension of high-danger conditions into winter demonstrate the effect of climate change on the seasonal pattern of fire danger across Iran's vegetation regions. Under both scenarios and in every season, the largest increase occurred in Khalij-Omani, followed by Irano-Turanian. The Zagros, Hyrcanian, and Arasbaran regions also experienced increases, although their magnitude varied. Thus, greater future fire danger would not be limited to central, southern, and eastern Iran; mountainous ecosystems in western, northern, and northwestern Iran would also be affected. Fire-monitoring, prevention, and management programs should therefore be revised in light of Iran's projected climate, with particular attention to mountainous regions. Beloiu et al. (2026) similarly concluded that the sensitivity of mountainous areas to fire would increase under stronger warming.

Fire occurrence is not governed by climate alone. Human population, land-use change, and the type and density of fuels also play decisive roles in ignition and spread. An increase in FWI does not therefore imply that fire occurrence will inevitably increase; rather, it indicates greater climatic potential for fire. Climate change in Iran is projected not only to increase mean FWI but also to expand the geographical area exposed to high fire danger.

Despite the importance of these findings, they should be interpreted in light of several limitations. These include the use of daily mean meteorological data rather than observations corresponding to local noon in the calculation of FWI

(Van Wagner, 1987; Matteo et al., 2025), uncertainties associated with climate models and emissions scenarios in projecting fire danger (Dupuy et al., 2020), and the exclusion of fuel-related and human factors (Van Vliet et al., 2024).

Declarations

Funding

This work is based upon research funded by the Iran National Science Foundation (INSF) under project No. 4037767.

Conflict of Interest

The authors declare that they have no conflict of interest.

Data Availability

The datasets used and/or analysed during the current study are available from the corresponding author on reasonable request.

References

Zarrin, A., & Dadashi Roudbari, A. (2022). Projection of precipitation intensity in Iran using a multi-model ensemble approach based on downscaled NEX-GDDP data. *Iranian Journal of Geophysics*, 16(1), 47-68. [In Persian].

Honareh, J., Choubin, B., & Heydari, M. (2023). The need to develop a social plan for combating forest and rangeland fires: Evidence from wildfire statistics in West Azerbaijan Province. *Proceedings of the Third National Conference on the Support and Protection of Iran's Forests and Rangelands*, Tehran, Iran. [In Persian].

Abram, N. J., Henley, B. J., Sen Gupta, A., Lippmann, T. J., Clarke, H., Dowdy, A. J., … & Boer, M. M. (2021). Connections of climate change and variability to large and extreme forest fires in southeast Australia. Communications Earth & Environment, 2(1), 8.

Arnell, N. W., Freeman, A., & Gazzard, R. (2021). The effect of climate change on indicators of fire danger in the UK. Environmental Research Letters, 16(4), 044027.

Azad, N., & Ahmadi, A. (2024). Assessment of CMIP6 models and multi-model averaging for temperature and precipitation over Iran. Scientific Reports, 14(1), 24165.

Barik, A., & Baidya Roy, S. (2023). Climate change strongly affects future fire weather danger in Indian forests. Communications Earth & Environment, 4(1), 452.

Beloiu, M., Loeillot, T., Griess, V. C., Poursanidis, D., & Petibon, F. (2026). Climate-driven upward spread of forest fires in European mountain regions. Nature Communications

Bento, V. A., Lima, D. C., Santos, L. C., Lima, M. M., Russo, A., Nunes, S. A., … & Soares, P. M. (2023). The future of extreme meteorological fire danger under climate change scenarios for Iberia. Weather and Climate Extremes, 42, 100623.

Bishop, C. H., & Abramowitz, G. (2013). Climate model dependence and the replicate Earth paradigm. Climate dynamics, 41, 885-900.

Bolan, S., Sharma, S., Mukherjee, S., Isaza, D. F. G., Rodgers, E. M., Zhou, P., … & Bolan, N. (2025). Wildfires under changing climate, and their environmental and health impacts. Journal of soils and sediments, 25(11), 3173-3197.

Bowman, D. M., Balch, J. K., Artaxo, P., Bond, W. J., Carlson, J. M., Cochrane, M. A., … & Pyne, S. J. (2009). Fire in the Earth system. science, 324(5926), 481-484.

Calheiros, T., Nunes, J. P., & Pereira, M. G. (2020). Recent evolution of spatial and temporal patterns of burnt areas and fire weather risk in the Iberian Peninsula. Agricultural and Forest Meteorology, 287, 107923.

Cardoso Pereira, S., Monteiro, N., Vaz, R., & Carvalho, D. (2024). High-resolution projections of future FWI conditions for Portugal according to CMIP6 future climate scenarios. Theoretical and Applied Climatology, 155(10), 9247-9272.

Carrillo, J., Pérez, J. C., Expósito, F. J., Díaz, J. P., & González, A. (2022). Projections of wildfire weather danger in the Canary Islands. Scientific reports, 12(1), 8093.

Debulois, S. G., Sun, M., & Li, M. (2026). Projection of fire weather index in Daxing'anling, Northeast China using a machine learning-based CMIP6 multi-model ensemble. Climatic Change, 179(3), 47.

Di Giuseppe, F., Pappenberger, F., Wetterhall, F., Krzeminski, B., Camia, A., Libertá, G., & San Miguel, J. (2016). The potential predictability of fire danger provided by numerical weather prediction. Journal of Applied Meteorology and Climatology, 55(11), 2469-2491.

Di Nunno, F., & Granata, F. (2025). Spatiotemporal analysis of the FWI over Europe and North Africa: Historical trends and climate projections under RCP4. 5 and RCP8. 5. Geoscience Frontiers, 102178.

Dupuy, J. L., Fargeon, H., Martin-StPaul, N., Pimont, F., Ruffault, J., Guijarro, M., … & Fernandes, P. (2020). Climate change impact on future wildfire danger and activity in southern Europe: a review. Annals of Forest Science, 77(2), 35.

Dupuy, J. L., Fargeon, H., Martin-StPaul, N., Pimont, F., Ruffault, J., Guijarro, M., … & Fernandes, P. (2020). Climate change impact on future wildfire danger and activity in southern Europe: a review. Annals of Forest Science, 77(2), 1-24.

Eyring V, Bony S, Meehl G A, Senior C A, Stevens B, Stouffer R J and Taylor K E 2016 Overview of the coupled model intercomparison project phase 6 (CMIP6) experimental design and organization Geosci. Model. Dev. 9 1937–58

Flannigan, M., Cantin, A.S., De Groot, W.J., Wotton, M., Newbery, A. and Gowman, L.M., 2013. Global wildland fire season severity in the 21st century. Forest Ecology and Management, 294, pp.54-61. https://doi.org/10.1016/j.foreco.2012.10.022

Gallo, C., Eden, J. M., Dieppois, B., Drobyshev, I., Fulé, P. Z., San-Miguel-Ayanz, J., & Blackett, M. (2022). Evaluation of CMIP6 model performances in simulating fire weather spatiotemporal variability on global and regional scales. Geoscientific Model Development Discussions, 2022, 1-31.

Ghazi, B., Salehi, H., Cheshami, M., Zeydalinejad, N., & Linh, N. T. T. (2025). Projection of climate change impact on main climate variables and assessment of the future of Köppen–Geiger climate classification in Iran. Acta Geophysica, 73(2), 2017-2027.

Haas, O., Prentice, I. C., & Harrison, S. P. (2026). Wildfires on a changing planet. Nature Communications.

He, Y., Zhou, Z., Im, E. S., & Kwon, H. H. (2025). Wildfire risk in a changing climate: Evaluating fire weather indices and their global patterns with CMIP6 multi-model projections. Weather and Climate Extremes, 48, 100751.

Hennessy, K., Lucas, C., Nicholls, N., Bathols, J., Suppiah, R., & Ricketts, J. (2005). Climate change impacts on fire-weather in south-east Australia. Climate Impacts Group, CSIRO Atmospheric Research and the Australian Government Bureau of Meteorology, Aspendale.

Jain, S., Salunke, P., Mishra, S. K., Sahany, S., & Choudhary, N. (2019). Advantage of NEX-GDDP over CMIP5 and CORDEX data: Indian summer monsoon. Atmospheric Research, 228, 152-160.

Jolly, W. M., Cochrane, M. A., Freeborn, P. H., Holden, Z. A., Brown, T. J., Williamson, G. J., &Bowman, D. M. J. S. (2015) Climate-induced variations in global wildfire danger from 1979 to 2013. Nature Communications, 6(1).

Jones, M. W., Abatzoglou, J. T., Veraverbeke, S., Andela, N., Lasslop, G., Forkel, M., … & Le Quéré, C. (2022). Global and regional trends and drivers of fire under climate change. Reviews of Geophysics, 60(3), e2020RG000726.

Koulelis, P. P., Proutsos, N., Solomou, A. D., Avramidou, E. V., Malliarou, E., Athanasiou, M., … & Petrakis, P. V. (2023). Effects of climate change on Greek forests: A review. Atmosphere, 14(7), 1155.

Lei X, Xu C, Liu F, Song L, Cao L, Suo N. Evaluation of CMIP6 Models and Multi-Model Ensemble for Extreme Precipitation over Arid Central Asia. Remote Sensing. 2023; 15(9):2376. https://doi.org/10.3390/rs15092376

Li, F., Song, X., Harrison, S. P., Marlon, J. R., Lin, Z., Leung, L. R., Schwinger, J., Marécal, V., Wang, S., Ward, D. S., Dong, X., Lee, H., Nieradzik, L., Rabin, S. S., and Séférian, R.: Evaluation of global fire simulations in CMIP6 Earth system models, Geosci. Model Dev., 17, 8751–8771, https://doi.org/10.5194/gmd-17-8751-2024, 2024.

Lucas-Borja, M. E., Peterson, C. L., & Stevens-Rumann, C. (2025). Managing pine forest ecosystems after fire: The need of being proactive under future uncertainty. Forest Ecology and Management, 598, 123188.

Mansouri Daneshvar, M.R., Ebrahimi, M. & Nejadsoleymani, H. An overview of climate change in Iran: facts and statistics. Environ Syst Res 8, 7 (2019).

Matteo, A., Garnés-Morales, G., Moreno, A., Ribeiro, A. F., Azorin-Molina, C., Bedia, J., … & Turco, M. (2025). Challenges in assessing Fire Weather changes in a warming climate. npj Climate and Atmospheric Science, 8(1), 284.

Matteo, A., Garnés-Morales, G., Moreno, A., Ribeiro, A. F., Azorin-Molina, C., Bedia, J., … & Turco, M. (2025). Challenges in assessing Fire Weather changes in a warming climate. npj Climate and Atmospheric Science, 8(1), 284.

Meng H, Di Z, Zhang W, Sun H, Tian X, Wang X, Xie M, Li Y. Spatiotemporal Analyses of High-Resolution Precipitation Ensemble Simulations in the Chinese Mainland Based on Quantile Mapping (QM) Bias Correction and Bayesian Model Averaging (BMA) Methods for CMIP6 Models. Atmosphere. 2025; 16(10):1133. https://doi.org/10.3390/atmos16101133

Miller, B. P., Fontaine, J. B., Tangney, R., McCaw, L., Cruz, M. G., & Hollis, J. J. (2024). Comment on 'Self-thinning forest understoreys reduce wildfire risk, even in a warming climate'. Environmental research letters, 19(6), 068001.

Ndalila, M. N., Lala, F., & Makindi, S. M. (2024). Community perceptions on wildfires in Mount Kenya forest: implications for fire preparedness and community wildfire management. Fire Ecology, 20(1), 92.

Nogherotto, R., Raffaele, F., Giuliani, G., & Coppola, E. (2026). Has the Fire Weather Index Emerged? Insights from Global and Regional Climate Models. Weather and Climate Extremes, 100861.

Novenko, E., Rudenko, O., Mazei, N., Kupriyanov, D., Andreev, R., Shatunov, A., … & Olchev, A. (2023). Effects of climate change and fire on the middle and late holocene forest history in yenisei siberia. Forests, 14(12), 2321.

Politi N, Vlachogiannis D, Sfetsos A, Gounaris N, Varela V(2023). Investigation of Fire Weather Danger under a Changing Climate at High Resolution in Greece. Sustainability; 15(3):2498.

Roshan, G., Ghanghermeh, A., Eshaghi, M. A., Sarli, R., & Grab, S. W. (2025). Spatiotemporal analysis of weather-related fire danger associated with climate change in the Zagros Mountains, Iran. Stochastic Environmental Research and Risk Assessment, 39(1), 55-80.

Ruosteenoja, K., & Jylhä, K. (2021). Projected climate change in Finland during the 21st century calculated from CMIP6 model simulations. Geophysica, 56(1), 39-69.

San-Miguel-Ayanz, J., & Ravail, N. (2005). Active fire detection for fire emergency management: Potential and limitations for the operational use of remote sensing. Natural Hazards, 35, 361-376.

Stocks, B.J.; Lawson, B.D.; Alexander, M.E.; Van Wagner, C.E.; McAlpine, R.S.; Lynham, T.J.; Dube, D.E. Canadian Forest Fire Danger Rating System: An overview. For. Chron. 1989, 65, 258–265.

Tebaldi, C., & Knutti, R. (2007). The use of the multi-model ensemble in probabilistic climate projections. Philosophical transactions of the royal society A: mathematical, physical and engineering sciences, 365(1857), 2053-2075.

Thrasher, B., Xiong, J., Wang, W., Melton, F., Michaelis, A., & Nemani, R. (2013). Downscaled climate projections suitable for resource management. Eos, Transactions American Geophysical Union, 94(37), 321-323.

Tian, X. R., Dai, X., Wang, M. Y., Zhao, F. J., & Shu, L. F. (2016). Forest fire risk assessment for China under different climate scenarios. Ying Yong Sheng tai xue bao= The Journal of Applied Ecology, 27(3), 769-776.

Türkan, S., Özel, G., Güney, C. O., Ünal, C., Şentürk, Ö., & Özkan, K. (2023). A New Approach to Determine the Influence of Weather Conditions on Forest Fire Risk in the Mediterranean Region of Türkiye. Mugla Journal of Science and Technology, 9(2), 1-10.

Van Vliet, L., Fyke, J., Nakoneczny, S., Murdock, T. Q., & Jafarpur, P. (2024). Developing user-informed fire weather projections for Canada. Climate Services, 35, 100505.

Van Wagner, C. E., & Pickett, T. L. (1985). Equations and FORTRAN program for the Canadian forest fire weather index system (Vol. 33).

Whittaker, T., Di Luca, A., Roberge, F., & Winger, K. (2025). Evaluating near-surface wind speeds simulated by the CRCM6-GEM5 model using AmeriFlux data over North America. Journal of Advances in Modeling Earth Systems, 17(3), e2024MS004666.

Xiao, Y., Zhang, X. and Ji, P., 2015. Modeling forest fire occurrences using count-data mixed models in qiannan autonomous prefecture of Guizhou Province in China. PloS one, 10(3), e0120621. https://doi.org/10.1371/journal.pone.0120621.